

Distinguishing Kilonovae from Binary Neutron Star and Neutron Star-Black Hole Mergers

ISH GUPTA ^{1,2,3} YUGESH BHOGE ⁴ RAHUL KASHYAP ⁴ AND MUKUL BHATTACHARYA ^{5,6,7}

¹*Department of Physics, University of California, Berkeley, CA 94720, USA*

²*Department of Physics and Astronomy, Northwestern University, 2145 Sheridan Road, Evanston, IL 60208, USA*

³*Center for Interdisciplinary Exploration and Research in Astrophysics (CIERA), Northwestern University, 1800 Sherman Ave, Evanston, IL 60201, USA*

⁴*Department of Physics, Indian Institute of Technology Bombay, Mumbai 400076, India*

⁵*Department of Physics; Department of Astronomy & Astrophysics; Center for Multimessenger Astrophysics, Institute for Gravitation and the Cosmos, The Pennsylvania State University, University Park, PA 16802, USA*

⁶*Department of Physics, Wisconsin IceCube Particle Astrophysics Center, University of Wisconsin, Madison, WI 53703, USA*

⁷*Department of Astronomy, Astrophysics and Space Engineering, Indian Institute of Technology Indore, Simrol, MP 453552, India*

ABSTRACT

Kilonovae from compact binary mergers are most informative when accompanied by a gravitational-wave signal, which can help identify the source as a binary neutron star (BNS) or a neutron star-black hole (NSBH) merger. However, future events will also be discovered serendipitously or through follow-up of other transients, without a confident identification of the progenitor. Hence, we ask whether the kilonova light curve alone can distinguish between these two progenitor channels. Using simulated BNS and NSBH populations together with semi-analytic light curve models, we compare their post-peak evolution across the optical *ugrizy* bands. The strongest contrast appears in the blue *u* band 2 days after peak and in the redder *i* band 10 days after peak. In the *u* band, typical BNS kilonovae decline by only ~ 1 mag within 2 days of peak, whereas NSBH kilonovae typically decline by $\gtrsim 3$ mag over the same interval. In the *i* band, the trend reverses for most of the population, with NSBH kilonovae evolving more slowly than BNS kilonovae. We attribute this behavior to differences in ejecta mass, opacity, and diffusion timescale between the two merger classes. Although the quantitative overlap is model-dependent, the qualitative distinction persists across model variations, identifying post-peak decline to be a viable diagnostic for inferring whether the source was a BNS or an NSBH merger.

1. INTRODUCTION

Compact binaries containing at least one neutron star (NS) can be prolific multi-messenger sources. As these systems inspiral and merge, they radiate gravitational waves (GWs) detected by the LIGO-Virgo-KAGRA (LVK) detectors (Abac et al. 2025b). They can also eject neutron-rich material through tidal disruption or contact at merger. The resulting outflows power electromagnetic (EM) transients across the spectrum, including optical and near-infrared kilonovae (KNe) (Li & Paczyński 1998; Kulkarni 2005; Metzger et al. 2010), gamma-ray bursts (GRBs) (Eichler et al. 1989; Narayan et al. 1992), and broadband afterglow emission (Rees & Mészáros 1992; Wijers et al. 1997; Sari et al. 1998). Whether and in what form these counterparts appear depend sensitively on the component masses, spin parameters, orbital configuration, and the NS equation of state (EOS), which together set the amount, composition, geometry, and velocity of the ejecta.

The potential of joint GW-EM observations was established by the binary neutron star (BNS) event GW170817 (Abbott et al. 2017a), which produced a rich suite of EM counterparts from gamma-ray to radio (Abbott et al. 2017b,c; Soares-Santos et al. 2017; Cowperthwaite et al. 2017; Nicholl et al. 2017; Chornock et al. 2017; Margutti et al. 2017; Alexander et al. 2017; Fong et al. 2017). Combined with precise GW constraints, GW170817 catalyzed advances in transient modeling and multi-messenger inference (Chornock et al. 2017; Villar et al. 2017; Radice et al. 2018b, 2020; Breschi et al. 2021; Gutiérrez et al. 2025), established BNS mergers as the progenitors of at least some short-duration GRBs (Rezzolla et al. 2010, 2011), and confirmed compact object mergers as sites of heavy element (*r*-process) nucleosynthesis (Lattimer & Schramm 1974; Symbalisty & Schramm 1982; Thielemann et al. 2017).

In contrast, although neutron star-black hole (NSBH) mergers have been reported by LVK (Abbott et al. 2021), and the sample has grown through the fourth

observing run (Abac et al. 2025b,c), no EM counterpart has been confidently associated with any NSBH event despite extensive follow-up campaigns (e.g., Anand et al. 2021; Ashkar et al. 2021; Kasliwal et al. 2020; Paterson et al. 2021; Abbasi et al. 2021; Ronchini et al. 2024; Paek et al. 2025). This gap leaves open questions on whether typical NSBH mergers eject enough mass to power observable KNe (Bhattacharya et al. 2019; Chattopadhyay et al. 2022), which binary configurations are EM-bright (Chattopadhyay et al. 2021; Biscoveanu et al. 2022; Gupta et al. 2023), whether NSBH mergers launch short or long-duration GRBs (Zhu et al. 2022; Gottlieb et al. 2023), and how much these mergers contribute to r -process enrichment (Saleem et al. 2025).

GW triggers provide critical information for EM counterpart search strategies. Signal-to-noise ratio accumulated during the inspiral phase can yield early-warning alerts with coarse localizations that enable rapid follow-up searches (Sachdev et al. 2020; Magee et al. 2021). In addition, GW parameter estimation constrains component masses and spins of binaries (Abbott et al. 2017a, 2021; Abac et al. 2024; Gupta 2024), which informs the expected EM phenomenology as well as the plausible source class between BNS and NSBH mergers (Chaudhary et al. 2024). Planned upgrades, such as A+ (Miller et al. 2015; Abbott et al. 2018), and proposed next-generation facilities such as Cosmic Explorer (Abbott et al. 2017d; Reitze et al. 2019; Evans et al. 2023; Gupta et al. 2024) and Einstein Telescope (Punturo et al. 2010; Hild et al. 2011; Branchesi et al. 2023; Abac et al. 2025a) promise more frequent joint detections (Zhu et al. 2021, 2023; Gupta 2023). However, with near-term A+ sensitivities, the network reach⁸ for BNS (NSBH) events is ~ 0.1 (~ 0.2) (Borhanian & Sathyaprakash 2024; Gupta et al. 2023), which is significantly lower than the redshifts at which state-of-the-art surveys such as the Vera C. Rubin Observatory (Ivezic et al. 2019; Cowperthwaite et al. 2019; Andreoni et al. 2022) and the Nancy Grace Roman Space Telescope (Hounsell et al. 2018; Chase et al. 2022; Andreoni et al. 2024) will detect KNe.

Efficient follow-up efforts also rely on GW-enabled sky localization and detector duty cycle. Two-detector baselines typically localize events to $\mathcal{O}(10^3)$ deg² (Fairhurst 2011), so simultaneous multi-detector GW observations are essential. Missed opportunities can result from single-detector triggers, as illustrated by the low mass NSBH candidate GW230529 (Abac et al. 2024), which may have produced a KN (Chandra et al. 2024; Kun-

numkai et al. 2025) but lacked a precise sky localization to enable targeted searches (Ronchini et al. 2024; Paek et al. 2025). The second detected BNS merger, GW190425 (Abbott et al. 2020), also faced similar challenges (Paek et al. 2024).

Given that present and future EM facilities will continue to discover KNe serendipitously (Andreoni et al. 2024), and in association with other transients such as GRBs (Tanvir et al. 2013; Rastinejad et al. 2022), we ask an intriguing question: in the absence of a GW detection, can the observation of KN alone indicate whether the progenitor was a BNS or an NSBH merger? Put differently, are there any observationally accessible differences between BNS and NSBH KN light curves that enable EM-only classification?

In this work, we model KN light curves for simulated BNS and NSBH populations with widely used semi-analytic prescriptions and numerical-relativity-calibrated fits. We assess whether these models predict observable differences between BNS and NSBH KNe that could enable EM-only source classification. We find that they do, as shown in Figure 1. Motivated by the relationship between the intrinsic luminosity and decay rate of Type Ia supernovae (Phillips 1993; Riess et al. 1998) and KNe (Kashyap et al. 2019), we introduce a distance-independent post-peak decline measure for KNe, defined as the difference between the peak KN magnitude and the magnitude after a fixed time in a given photometric band. We find that the post-peak decline in the blue (u) band provides a strong avenue for separating the two merger classes, with NSBH KNe declining faster than BNS KNe. This trend remains robust to variations in the assumptions of the astrophysical population, the NS EOS, and several parameters of the KN model. We also identify differences in the red (i) band light curve, where most NSBH KNe decline more slowly after peak than BNS KNe, although this distinction is more model-dependent. These results establish post-peak photometric decline as a promising EM-only probe of the progenitor, and motivate future efforts to revisit these regions of parameter space using comprehensive simulations.

The rest of the paper is organized as follows. Section 2 presents our semi-analytic framework for modeling BNS and NSBH KNe, along with its main assumptions and caveats. In Section 3, we compare the post-peak decline of the two merger classes and identify the bands and timescales where their KN emission differs most clearly. We then assess the robustness of these differences to variations in the astrophysical population priors (Section 3.1), NS EOS (Section 3.2), and ejecta-model parameters (Section 3.3). We summarize our results and

⁸ In Borhanian & Sathyaprakash (2024) and Gupta et al. (2023), reach is defined as the redshift at which 50% of mergers are detected.

discuss their implications in Section 4. Additional technical details are collected in the Appendix.

2. KILONOVA MODELING

KNe are powered by the radioactive decay of r -process nuclei in neutron-rich ejecta, produced by the disruption of the NS in BNS and NSBH mergers. The decay of these radioactive heavy elements yields high-energy gamma rays that scatter off free electrons and convert to UV/optical/IR photons, generating transients in these bands. While both BNS and NSBH mergers can synthesize heavy elements, the electron fraction (Y_e) and lanthanide distribution can differ between ejecta components and between merger types (for example, see Table 1 in Ekanger et al. (2023)). This directly impacts the effective opacity and the color evolution of the transient.

At early times, the ejecta is optically thick, so deposited radioactive energy is trapped, and the luminosity is regulated by photon diffusion. As the ejecta expands and rarefies, the optical depth decreases and radiation begins to escape, producing a rise to peak followed by a decline that increasingly tracks the declining radioactive power. The time to peak can be expressed by the geometric mean of two characteristic timescales: the expansion timescale, $\tau_{exp} = R/v$, and the diffusion timescale, $\tau_{diff} = \kappa M/\beta cR$ (Metzger 2020). Here, κ denotes the opacity of the ejecta component, R is the length scale associated with the ejecta component, and $\beta = 13.8$ is a dimensionless constant that encodes the geometric structure of the ejecta (Chatzopoulos et al. 2012). The ejecta mass M and velocity v are set by the binary system parameters and the nuclear EOS. In general, larger M and κ result in slower evolution of the light curve, while the latter also results in redder emission (Barnes & Kasen 2013).

We model KN emission within the Arnett–Chatzopoulos–Villar framework (Arnett 1982; Chatzopoulos et al. 2012; Villar et al. 2017), which maps ejecta masses, velocities, and opacities to band-wise light curves. For BNS mergers, we adopt the three-component prescription of Villar et al. (2017), treating lanthanide-rich “red” component ($\kappa = 10 \text{ cm}^2 \text{ g}^{-1}$), intermediate-opacity “purple” component ($\kappa = 3 \text{ cm}^2 \text{ g}^{-1}$), and lanthanide-poor “blue” component ($\kappa = 0.5 \text{ cm}^2 \text{ g}^{-1}$) as independent diffusion zones. For each BNS, the dynamical ejecta and remnant disk outflow masses and velocities are determined from the NS masses and EOS using numerical-relativity-calibrated fits from Nedora et al. (2022). We then distribute the total ejecta among the three opacity components with fixed mass fractions $(f_{\text{red}}, f_{\text{purple}}, f_{\text{blue}}) = (0.2, 0.6, 0.2)$. The model is evolved separately for each component to

obtain its luminosity as a function of time. The total bolometric light curve is the sum of the three components, and the corresponding band fluxes are obtained by summing the component contributions in each filter.

In NSBH mergers, EM counterparts are produced only if the NS is tidally disrupted before reaching the BH’s innermost stable circular orbit (ISCO). Consequently, in addition to the NS mass and EOS, the existence and amount of ejecta depend strongly on the BH mass and spin. For sufficiently massive BHs, the NS typically plunges with little or no disruption. By contrast, a rapidly spinning BH with spin aligned to the orbital angular momentum reduces the effective ISCO radius and enhances tidal disruption, increasing both the remnant disk mass and the unbound outflows. For disrupted NSBH systems, we adopt a two-component KN model consisting of a lanthanide-rich dynamical component and a remnant disk outflow (disk wind) component. We evolve each component as an independent one-zone diffusion region, characterized by its ejecta mass, expansion velocity, and effective opacity. The dynamical ejecta is expected to be highly neutron-rich and, consequently, lanthanide-rich, while disk outflows typically synthesize lighter r -process nuclei, albeit with a lanthanide fraction that can vary with the disk properties and the central BH (Just et al. 2015; Wu et al. 2016; Lippuner et al. 2017). Consistent with this picture, we adopt $Y_e \sim 0.05 - 0.1$ ($\kappa \sim 37 \text{ cm}^2 \text{ g}^{-1}$) for dynamical ejecta, and $Y_e \sim 0.1 - 0.5$ ($\kappa \sim 2 - 37 \text{ cm}^2 \text{ g}^{-1}$, see Appendix A.1.2 for details) for disk outflows (Ekanger et al. 2023).

For each NSBH binary, the ejecta-component masses and velocities are determined from numerical-relativity-calibrated fitting formulae that capture the dependence on mass ratio, BH spin, and NS compactness (Foucart et al. 2018; Krüger & Foucart 2020; Raaijmakers et al. 2021). We compute bolometric light curves for the dynamical and disk wind components within the same Arnett–Chatzopoulos–Villar framework used for BNS mergers, and obtain the total emission by summing the component contributions. The full set of fitting formulae for both BNS and NSBH mergers are provided in Appendix A.

To obtain band-limited light curves from the bolometric emission, we assume the ejecta radiates approximately as a blackbody. At each time step, we infer an effective photospheric radius and temperature from the luminosity and expansion, use these to construct the corresponding spectral energy distribution, and evaluate the spectral flux density at the effective wavelength of different photometric filters. We then convert the resulting fluxes to AB magnitudes, yielding band-wise

light curves directly comparable to survey photometry. We generate light curves in the optical *ugrizy* bands, the details of which are mentioned in Appendix A.1.3.

There are several caveats to our KN modeling. First, we estimate ejecta masses and velocities using analytical fits to numerical relativity simulations. These fits can cause errors of at least $\mathcal{O}(10\%)$ in the predicted ejecta masses (Krüger & Foucart 2020; Foucart et al. 2018), and in some regions of the parameter space, they can also be ill-conditioned (Nedora et al. 2022). Moreover, many of the underlying simulations follow the post-merger evolution for only tens of milliseconds and do not capture the full accretion evolution of the remnant disk and its long-lived outflows, largely due to computational cost. Some of these simulations also use approximate neutrino treatments rather than full neutrino transport, which can affect the predicted Y_e distribution and, in turn, the opacities and heating rates that shape the KN light curves.

Second, the adopted prescription for radioactive heating introduces additional uncertainty (Bulla 2023; Sarin & Rosswog 2024). In this work, we use a common functional form for the heating rate across both BNS and NSBH mergers. In reality, however, the isotopic abundance pattern can differ between the ejecta of the two merger classes, leading to differences in both the normalization and the temporal evolution of the heating. Third, we assume isotropic emission and neglect viewing-angle effects arising from aspherical ejecta geometry and composition gradients. In realistic systems, both the angular distribution of the ejecta and angle-dependent opacities can imprint substantial anisotropy on the luminosity and color evolution of the transient (Klion et al. 2020; Heinzl et al. 2020; Darbha & Kasen 2020; Shingles et al. 2023).

Uncertainties in atomic transition data introduce a further source of error through the inferred ejecta opacities. At early times, these uncertainties typically translate to errors of less than about one magnitude in Rubin’s *r* and *y* bands, as well as in JWST observations near $\sim \mu\text{m}$, with the corresponding impact on bolometric magnitudes remaining below the $\sim 20\%$ level (Brethauer et al. 2024). However, at later times, revisions to atomic datasets and variations in thermalization efficiency can produce substantially larger discrepancies.

While we test the robustness of our conclusions against several modeling assumptions (see, for e.g., Section 3.3 and Appendix A.1.1), a more definitive assessment will ultimately require a dedicated (albeit computationally prohibitive) set of high-resolution simulations with self-consistent treatment of nucleosynthesis, together with full radiative transfer. This work shows

that, within widely used semi-analytic prescriptions, BNS and NSBH KNe are distinguishable, and motivates future efforts to study these unexplored regions of parameter space with more sophisticated models.

3. DIFFERENTIATING BETWEEN BNS AND NSBH KILONOVAE

To quantify how KNe from BNS and NSBH mergers differ, we simulate populations of both classes and generate bandwise light curves using the framework summarized in Section 2 and delineated in Appendix A. For the fiducial BNS population, we draw the primary mass m_1 uniformly from $\mathcal{U}(1, 2.5) M_\odot$ and the secondary mass $m_2 \in \mathcal{U}(1, m_1) M_\odot$. For NSBH binaries, we sample the BH mass $m_{\text{BH}} \in \mathcal{U}(2.5, 12) M_\odot$, the NS mass $m_{\text{NS}} \in \mathcal{U}(1, 2.5) M_\odot$, and the dimensionless BH spin $a_{\text{BH}} \in \mathcal{U}(-0.75, 0.75)$. All systems are placed at a fixed luminosity distance of 200 Mpc. To capture the dependence on EOS, we repeat the analysis for three representative choices: SLy (Douchin & Haensel 2001), APR4 (Akmal et al. 1998) and DD2 (Banik et al. 2014), spanning soft to stiff behavior. Although our population permits NS masses up to $2.5 M_\odot$ (near the maximum supported by DD2), light curves are generated only for NS masses consistent with the EOS under consideration. We also enforce $m_{\text{BH}, \text{min}} = 2.5 M_\odot$, deliberately targeting the regime in which a low mass BH and a high mass NS can be difficult to distinguish using GW tidal information alone (Golomb et al. 2024; Dhani et al. 2025). In such cases, systematic differences in the KN photometric evolution offer an EM-only route to source classification.

Our strategy is to statistically compare KNe from BNS and NSBH mergers using observables that are directly measurable from survey photometry. We characterize each light curve by its peak AB magnitude in a given band, $m_{\text{AB}}^{\text{peak}}$, and its post-peak decline over a fixed time, $m_{\text{AB}}^{\text{peak}} - m_{\text{AB}}^{\text{peak}+\Delta t}$, with $\Delta t = 1, 2, 5, 10$, and 15 days. This parameter captures the decline rate while remaining insensitive to luminosity distance. This approach is inspired by Kashyap et al. (2019), who showed that, similar to Type IA supernovae, the bolometric decline rate for BNS KNe correlates with their intrinsic bolometric luminosity, suggesting that measuring post-peak decline can help in standardizing KNe.

The temporal evolution across all modeled bands is shown in Figure 7 (Appendix C). Guided by those trends, we focus on two particular cases: the decline in the blue *u* band 2 days after peak, and the red *i* band 10 days after peak. The delay time is chosen empirically and determined by examining the ensemble of light curves. Figure 1 shows the probability densities of $m_{\text{AB}}^{\text{peak}} - m_{\text{AB}}^{\text{peak}+\Delta t}$ in these bands for BNS and NSBH

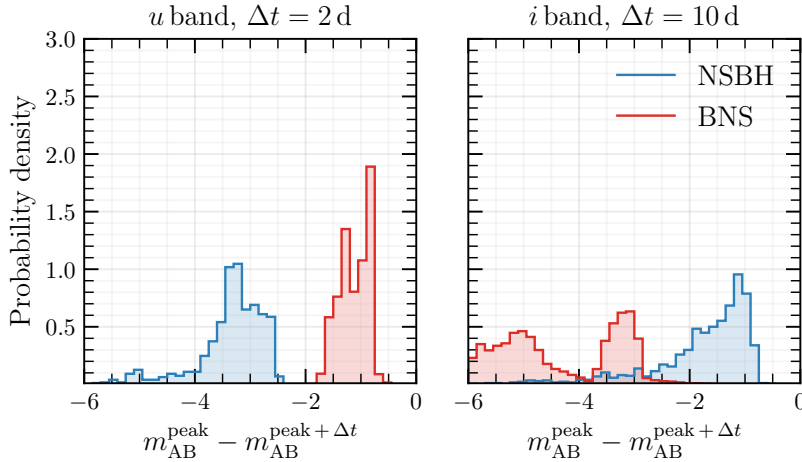


Figure 1. Distribution of the post-peak decline $m_{\text{AB}}^{\text{peak}} - m_{\text{AB}}^{\text{peak}+\Delta t}$ for KNe from BNS (red) and NSBH (blue) mergers. Left: u band with $\Delta t = 2$ d. Right: i band with $\Delta t = 10$ d. Each histogram combines samples from all three NS EOS considered. We find the two populations to be well separated in the u band, with some overlap in the i band.

systems, combining samples across the three EOSs. In both filters, the two merger classes populate distinct regions of this post-peak decline parameter space. In the u band, NSBH KNe decay substantially faster than BNS KNe: typical BNS events dim by ~ 1 mag within 2 days of peak, whereas NSBH events dim by $\gtrsim 3$ mag over the same interval. In the i band, the trend is reversed for most of the population, with NSBH KNe exhibiting a slower post-peak decline ($\sim 1 - 2$ mag) than BNS KNe ($\sim 3 - 5$ mag) over 10 days.

These differences can be understood in terms of the ejecta properties that control diffusion time and color evolution: the ejecta mass, velocity and effective opacity. In the BNS model, the low-opacity blue component contributes significantly to early-time blue emission and is assigned $\kappa \simeq 0.5 \text{ cm}^2 \text{ g}^{-1}$, while the purple and red components have higher opacities and dominate progressively later times. For DD2, the ejecta masses span $\sim 0.003\text{--}0.01 M_{\odot}$ in the red and blue components and $\sim 0.01\text{--}0.03 M_{\odot}$ in the purple component. In the NSBH model, only a subset of binaries undergo NS disruption outside ISCO and produce non-negligible ejecta; for those systems, the ejecta is typically more neutron-rich and therefore more opaque. For DD2, the disrupted NSBH systems in our population have median dynamical ejecta and disk wind masses of $\sim 0.025 M_{\odot}$ and $\sim 0.013 M_{\odot}$, respectively, with both components assigned substantially larger effective opacities than the BNS blue component. The higher opacity accelerates the decline of blue emission, yielding the rapid u band decline observed in our simulated NSBH KNe. At the same time, larger masses in high opacity components increase the characteristic diffusion time and sustain red emission for longer, naturally producing a slower decline

in the i band for most NSBH events with non-negligible ejecta mass.

Beyond modeling systematics, the degree of separation between BNS and NSBH KNe can also depend on the assumptions used to construct the underlying binary populations and determine ejecta properties. In the remainder of this section, we test the robustness of the inferred KN distinguishability under variations of these inputs. In Section 3.1, we repeat the analysis for alternative, astrophysically motivated BNS and NSBH populations and check how the distinguishability of the post-peak decline distribution changes. In Section 3.2, we isolate EOS effects by comparing the separation in the post-peak decline distributions across the three NS EOS choices. Finally, in Section 3.3, we vary the assumed Y_e (and, hence, the opacity) for the NSBH dynamical ejecta and disk wind components, and mass and velocity of the three BNS ejecta components, and reassess the resulting light curve differences.

3.1. Impact of astrophysical population

To assess whether our result depends on population assumptions, we repeat the analysis using additional, astrophysically motivated priors for BNS and NSBH masses and spins. The adopted mass distributions are summarized in Table 1. For BNS systems, we consider a single Gaussian motivated by Galactic double NS measurements (Farrow et al. 2019), and a double-Gaussian mixture that incorporates additional pulsar constraints (Antoniadis et al. 2016; Özel & Freire 2016) and follows Gupta et al. (2024). For NSBH systems, we adopt a ‘‘Gaussian + Uniform’’ prescription in which the BH mass is drawn from a Gaussian distribution motivated by the detected NSBH sample (Biscoveanu et al. 2022; Abac et al. 2024), while the NS mass remains uniform.

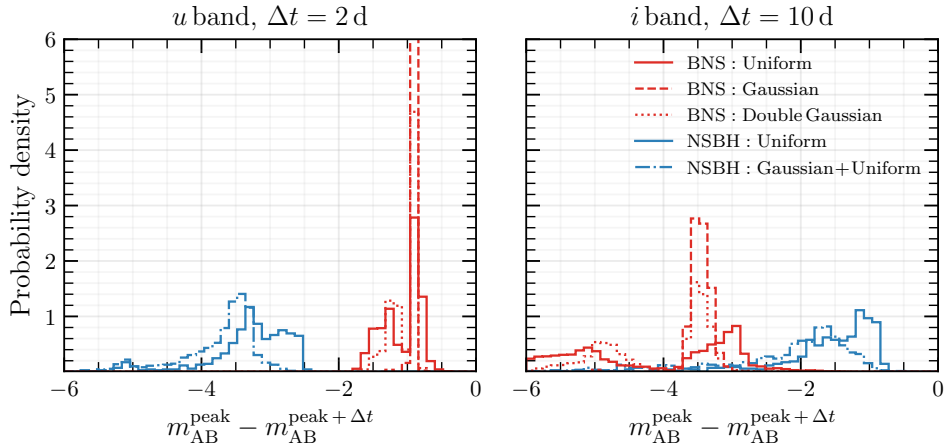


Figure 2. Same as Figure 1, but varying the astrophysical population priors for BNS and NSBH mergers while fixing the EOS to DD2. The separation in the u band plot is largely insensitive to the adopted population. In the i band, the “Gaussian + Uniform” NSBH prior shows slightly higher overlap with the BNS distributions.

We assume NSs to be non-spinning, and draw BH spins from $a_{\text{BH}} \sim \mathcal{N}(0, 0.2)$, to reflect the preference for low spins suggested by current detections (Biscoveanu et al. 2022). The NS EOS is fixed to DD2.

Population	$m_1 (M_\odot)$	$m_2 (M_\odot)$
BNS		
Uniform	$\mathcal{U}(1, 2.5)$	$\mathcal{U}(1, m_1)$
Gaussian	$\mathcal{N}(1.33, 0.9)$	
Double Gaussian	$0.64 \times \mathcal{N}(1.33, 0.9) + 0.36 \times \mathcal{N}(1.8, 0.3)$	
NSBH		
Uniform	$\mathcal{U}(2.5, 12)$	$\mathcal{U}(1, 2.5)$
Gaussian+Uniform	$\mathcal{N}(5, 1)$	$\mathcal{U}(1, 2.5)$

Table 1. Parameters describing the BNS and NSBH mass distributions considered in Section 3.1. $\mathcal{U}(a, b)$ denotes a uniform distribution between a and b , and $\mathcal{N}(\mu, \sigma)$ denotes a Gaussian distribution with mean μ and standard deviation σ . For all distributions, we enforce $m_1 > m_2$.

Figure 2 compares the resulting post-peak decline distributions with those obtained for the fiducial “Uniform” populations. As expected, the “Gaussian” populations generally produce narrower distributions than their “Uniform” counterparts, since they occupy a more restricted region of the parameter space. Overall, however, the separation between BNS and NSBH KNe persists under these changes in population priors. This robustness is especially evident in the u band, where NSBH events continue to occupy the rapidly declining region with little overlap with the BNS population.

For BNS mergers, the “Gaussian” and “Double Gaussian” populations contain fewer systems with $m_{\text{NS}} \lesssim 1.2 M_\odot$ and $m_{\text{NS}} \gtrsim 2 M_\odot$. As a result, their i band distributions lack both the fastest-declining ($\lesssim -6$ mag)

and the slowest-declining ($\gtrsim -3$ mag) tails seen in the fiducial “Uniform” population (cf. Figure 6 in Appendix B). For NSBH mergers, the “Gaussian + Uniform” population shows somewhat greater overlap with the “Uniform” BNS distribution in the i band, reflecting a shift toward faster post-peak decay. This behavior arises because the “Gaussian + Uniform” prescription concentrates BH masses around $\sim 5 M_\odot$. Relative to the fiducial “Uniform” prior, this increases the fraction of moderately mass-symmetric systems, but decreases the abundance of the most ejecta-producing binaries: near-equal-mass NSBH systems with $m_{\text{BH}}/m_{\text{NS}} \lesssim 2$ and large aligned BH spins. The “Uniform” NSBH prior, although it includes many highly mass-asymmetric binaries that do not disrupt, still retains more of this strongly ejecta-producing tail. Consequently, among systems that produce non-negligible ejecta, the “Gaussian + Uniform” population is weighted toward smaller ejecta masses and shorter diffusion timescales, leading, on average, to faster fading in both the u and i bands.

3.2. Impact of the NS equation of state

The EOS sets the NS compactness, which is an important parameter for tidal disruption and mass ejection. More compact NSs are harder to disrupt and, when disrupted, tend to produce less ejecta. Since the KN decline rate is sensitive to ejecta mass and opacity, EOS variations can alter the post-peak decline distribution. Hence, we repeat the analysis for the fiducial “Uniform” BNS and NSBH populations under each of the three EOSs and reassess the BNS–NSBH separability.

Among our EOS choices, APR4 generally yields the most compact (softest) NSs, followed by SLy, while DD2 produces the least compact (stiffest) NSs. The resulting trends in ejecta production follow this ordering. For

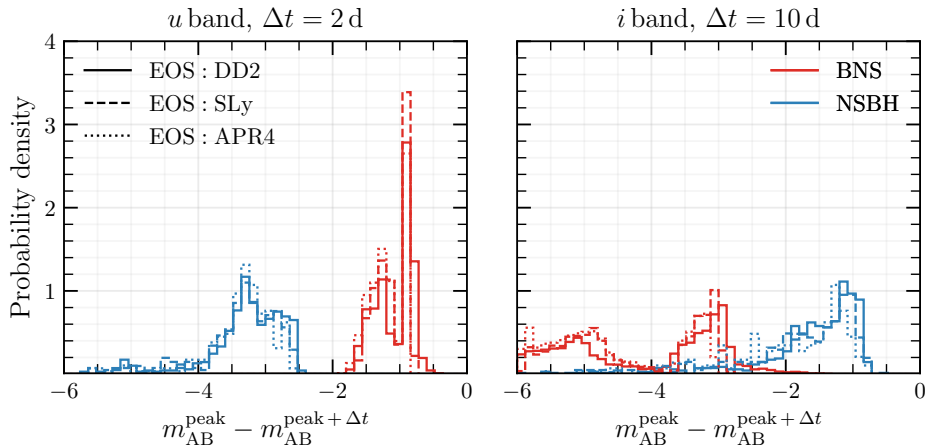


Figure 3. Same as Figure 1, but shown separately for each EOS. Varying the EOS produces only a small shift in the post-peak decline distributions and does not significantly change the separability between BNS and NSBH KNe in either band.

BNS mergers, DD2 yields the largest ejecta masses on average, followed by SLy and then APR4. For NSBH mergers, the EOS also affects the disruption fraction, because compactness enters directly into the criterion for disruption outside the BH ISCO in the calibrated fits. In our simulated NSBH population, the fraction of systems with non-negligible ejecta is $\sim 11\%$ for DD2, $\sim 6\%$ for SLy, and $\sim 4\%$ for APR4.

Figure 3 shows the resulting post-peak decline distributions in the u and i bands for each EOS. As we move from DD2 to APR4, both the BNS and NSBH populations shift mildly toward faster KN decay in both bands, consistent with smaller ejecta masses and shorter diffusion times for more compact stars. Importantly, this shift is subdominant to the separation between merger classes: the u band continues to show clear separation between BNS and NSBH KNe, while the i band separation persists with comparable overlap across EOS choices. We conclude that, within our modeling assumptions, the proposed post-peak decline criteria are reasonably robust to EOS uncertainty.

3.3. Impact of model parameters

Finally, we examine how uncertainties in the ejecta composition, opacity, and characteristic velocity affect the BNS–NSBH separation in the post-peak decline distribution. Throughout this analysis, we keep the astrophysical population fixed to the fiducial “Uniform” prior and adopt DD2 as the EOS for both BNS and NSBH systems.

For BNS mergers, we vary the allocation of the total unbound ejecta mass among the blue, purple, and red components from the fiducial fractions $f_m = \{0.2, 0.6, 0.2\}$ to $f_m = \{0.26, 0.60, 0.14\}$. The latter choice is motivated by the component-wise ejecta masses inferred for the KN associated with GW170817 (Villar

et al. 2017). In the fiducial model, all three components are assigned the same characteristic velocity. In the alternate model, however, we scale the velocities of the blue, purple, and red components as $\{1, 0.6, 0.5\}$ times the ejecta velocity inferred from the numerical-relativity-calibrated fits (see Appendix A.1.1). This ordering, in which the blue component evolves fastest and the red component slowest, is again consistent with the phenomenology inferred from GW170817 (Villar et al. 2017).

For NSBH mergers, we instead vary the electron fraction, and hence the opacity, of the ejecta components. As discussed in Section 2, the dynamical ejecta is expected to be highly neutron-rich and have low Y_e , while the disk outflow is expected to be less neutron-rich and have lower opacity. We vary the electron fraction of the dynamical ejecta from $Y_e = 0.1$ to $Y_e = 0.05$, and that of the disk wind from the fiducial value $Y_e = 0.3$ to $Y_e = \{0.1, 0.5\}$ (Ekanger et al. 2023). Using the fits to the opacity data from Tanaka et al. (2020), these values correspond to $\kappa = \{36.95, 36.82, 3.59, 1.98\} \text{ cm}^2 \text{ g}^{-1}$ for $Y_e = \{0.05, 0.1, 0.3, 0.5\}$, respectively (see Appendix A.1.2). Since the fitted opacity changes only minimally between $Y_e = 0.05$ and 0.1 , varying the composition of the dynamical ejecta within this range has a negligible impact on the resulting KN light curves. Thus, we focus on the effect of varying the disk wind composition.

Figure 4 shows the resulting changes in the post-peak decline distributions. For BNS mergers, the reduced velocities of the purple and red components in the alternate model slow the expansion, leading to less rarefied ejecta and more slowly evolving emission in the i band. By contrast, the u band distributions are only weakly affected, since they are dominated by the blue component,

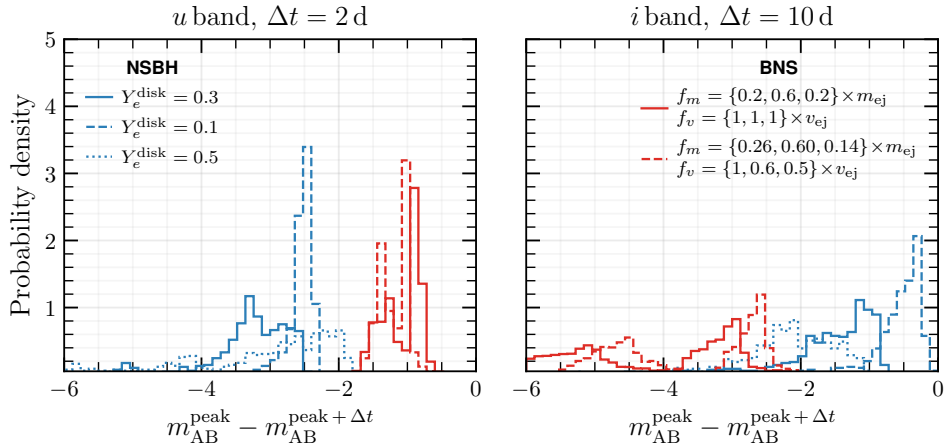


Figure 4. Same as Fig. 1, but illustrating the impact of variations in the ejecta-model assumptions for the fiducial “Uniform” populations with the DD2 EOS. For BNS mergers, we vary the allocation of the total unbound ejecta mass, m_{ej} , among the blue, purple, and red components from the fiducial fractions $f_m = \{0.2, 0.6, 0.2\}$ to $f_m = \{0.26, 0.60, 0.14\}$, and also modify the characteristic ejecta velocities, v_{ej} , of these components. For NSBH mergers, we instead vary the electron fraction of the disk wind ejecta, changing the fiducial value $Y_e = 0.3$ (corresponding to $\kappa \sim 3.6 \text{ cm}^2 \text{ g}^{-1}$) to $Y_e = 0.1$ ($\kappa \sim 37 \text{ cm}^2 \text{ g}^{-1}$) and $Y_e = 0.5$ ($\kappa \sim 2 \text{ cm}^2 \text{ g}^{-1}$).

whose velocity remains unchanged and whose emission peaks and decays on short timescales.

For NSBH mergers, the disk wind electron fraction strongly alters the color evolution through the opacity. The $Y_e^{\text{disk}} = 0.5$ case corresponds to the lowest opacity disk wind and, therefore, to a bluer KN. In this case, the emission shifts to shorter wavelengths, causing the i band light curve to decay more rapidly while the u band decay becomes slower relative to the fiducial $Y_e^{\text{disk}} = 0.3$ model. As a result, this case shows increased overlap with the alternate BNS model in the i band and reduced separation in the u band, although the two merger classes remain distinguishable.

The opposite trend is seen for $Y_e^{\text{disk}} = 0.1$, which corresponds to a much higher opacity disk wind and, consequently, a redder KN. In the i band, this produces very slowly declining light curves and the largest separation from the BNS population. In the u band, however, the difference relative to the fiducial $Y_e^{\text{disk}} = 0.3$ case is more modest. Although the $Y_e^{\text{disk}} = 0.1$ models are initially the dimmest in the blue and exhibit rapid early decline, the ejecta soon cools to the imposed temperature floor associated with recombination, at which point the opacity drops and the color evolution becomes nearly time-independent (Barnes & Kasen 2013). In the semi-analytic framework adopted here, this recombination temperature floor flattens the subsequent color evolution and prevents the u band light curves from continuing to decay rapidly. The details are described in Appendix A.1.3.

Overall, these variations show that the precise location of the BNS and NSBH populations in the post-peak de-

cline distribution depends on the ejecta modeling, particularly through the opacities and velocities assigned to the components. Nevertheless, the qualitative picture remains the same. Across the model variations considered here, BNS and NSBH KNe continue to populate systematically different post-peak decline distributions, with the separation in the bluer bands remaining especially robust, while the redder band distinction is more sensitive to assumptions about the composition and velocity structure of the ejecta. We conclude that, although the precise degree of separation in the post-peak decline distribution is model-dependent, the existence of observationally accessible differences between BNS and NSBH KNe is not an artifact of a single fiducial prescription.

4. CONCLUSIONS

Kilonovae (KNe) are optical and near-infrared transients powered by the radioactive decay of freshly synthesized r -process nuclei in neutron-rich ejecta. They were first identified as counterparts to some short GRBs, pointing to an origin in compact binary mergers. In particular, the merger of two NSs, or the tidal disruption of a NS by a BH, can eject neutron-rich matter under conditions favorable for heavy-element nucleosynthesis. This picture was confirmed by GW170817, a BNS merger that was accompanied by both a short GRB and a KN. However, no comparably secure association has yet been established for an NSBH merger.

A practical consequence is that the progenitor class of a KN may not always be known. This is especially relevant as optical surveys, like the Vera C. Rubin Observa-

tory and the Nancy Grace Roman Space Telescope, begin to probe beyond the effective multi-messenger reach of present GW networks, and because even GW-detected systems can remain difficult to classify in parts of the BNS–NSBH parameter space. This motivates the central question of this work: can one infer the progenitor class of a KN from the EM signal alone? Using simulated populations and semi-analytic light curve models calibrated to numerical simulations, we find that BNS and NSBH mergers do exhibit statistically different photometric evolution, opening a path toward EM-only source classification.

To quantify these differences, we compare BNS and NSBH KNe across the optical *ugrizy* bands using the post-peak decline distributions, constructed from the peak AB magnitude in a given band and the change in magnitude over a fixed interval after peak. This quantity is directly measurable from survey photometry, and the post-peak decay itself is independent of luminosity distance. Examining the full set of modeled bands, we find that the clearest separation appears in the blue *u* band 2 days after peak and in the redder *i* band 10 days after peak. In the *u* band, typical BNS KNe fade by only ~ 1 mag within 2 days of peak, whereas NSBH KNe typically fade by $\gtrsim 3$ mag over the same interval. In the *i* band, the trend is reversed for most of the population: NSBH KNe generally decline more slowly over 10 days than BNS KNe. This behavior follows from the ejecta properties that control the KN timescale and color evolution. In BNS mergers, the early blue emission receives a substantial contribution from the low opacity component, allowing the *u* band light curve to remain comparatively bright after peak. By contrast, ejecta-producing NSBH mergers typically contain more neutron-rich material with larger effective opacities in both the dynamical and disk wind ejecta, which suppresses blue emission and drives a more rapid post-peak decline in the *u* band. At the same time, these higher opacity components for NSBH events increase the diffusion time and shift more of the emission to later times and redder wavelengths, leading to a slower evolution in the *i* band compared to BNS KNe.

We tested how robust this separation in the post-peak decline distribution is to several classes of assumptions. First, changing the astrophysical population priors does not erase the difference between BNS and NSBH KNe. Our fiducial “Uniform” populations are already intentionally broad and agnostic, spanning a wide range of masses and spins, yet they still show clear separation, particularly in the *u* band. Adopting more astrophysically motivated priors generally narrows the distributions and, over much of the parameter space, pre-

serves or even strengthens the contrast between BNS and NSBH systems.

Second, varying the NS equation of state changes the NS compactness and, hence, the amount of ejecta produced. This effect is especially important for NSBH mergers, where more compact NSs are less likely to disrupt outside the BH’s innermost stable circular orbit and less likely to produce an observable KN. Considering NSBH systems that produce non-negligible ejecta, the relative placement of the BNS and NSBH populations in the post-peak decline distribution changes only slightly. Softer equations of state, corresponding to more compact NSs, generally yield smaller ejecta masses and faster evolution in both the *u* and *i* bands, but they do not significantly alter the separation between the two merger classes.

Third, we varied model parameters that directly control the KN color and diffusion timescale, including the mass and velocity of the BNS ejecta components, and the opacity of the NSBH disk wind. These changes shift the distributions in ways that are broadly consistent with physical expectations. Lower opacity NSBH disk winds produce bluer KNe, leading to more persistent blue band emission and more rapidly declining red band light curves, while higher opacity winds sustain redder light curves for longer. Likewise, assigning lower velocities to the BNS’s purple and red ejecta components causes ejecta to expand and rarefy more slowly, increasing the effective diffusion timescale and slowing the post-peak decay in the *i* band. Even so, these variations do not qualitatively alter the main result: across the model space explored here, BNS and NSBH KNe continue to occupy systematically different regions in the post-peak decline distribution.

These conclusions should be interpreted with appropriate caution. Our modeling relies on semi-analytic light curve prescriptions and simulation-calibrated ejecta fits, inheriting uncertainties from the underlying numerical simulations, fitting routines, heating rate prescriptions, opacity estimates, and neglecting viewing-angle dependence and detailed radiative transfer. We explicitly tested the stability of our results against several assumptions, but a definitive EM-only classification framework will ultimately require a much larger suite of high-resolution simulations with self-consistent neutrino transport, composition-dependent heating, and full radiative transfer. Even with these caveats, the central result is clear: within widely used models, BNS and NSBH KNe exhibit systematically different photometric evolution. The persistence of this separation across population priors, NS equation of state choices, and ejecta-model variations shows that the prospect of EM-only

source classification is not tied to any one particular prescription, but instead reflects a broader physical trend that merits detailed follow-up with state-of-the-art simulations.

If these trends persist under more sophisticated modeling, their implications are significant. Current KN datasets are generally too sparse to apply this framework, especially for events whose light curves have not informed the semi-analytic prescriptions used here. That situation may change rapidly with facilities such as Rubin and Roman, which are expected to discover larger samples of KNe, including better-sampled counterparts to short gamma-ray bursts and GW events. In that regime, the post-peak decline behavior identified here could help infer the likely nature of the underlying binary even when no GW information is available. The same is relevant when a GW signal is present but not decisive. At current detector sensitivities, low mass BHs can be difficult to distinguish from heavy NSs, and such systems are explicitly included in our broad NSBH population. Our results indicate that KNe of such low mass NSBHs can still differ appreciably from those of BNS mergers. If confirmed, this would provide an additional route to source classification, with direct implications for the maximum NS mass and the NS equation of state. More broadly, robust identification of BNS and NSBH KNe would also help address open questions about the relative contribution of different compact binary channels to Galactic r -process enrichment, and about whether NSBH mergers preferentially power short- or long-duration GRBs.

The natural next step is to test these predictions using more complex ejecta and heating prescriptions, explicit radiative transfer, and viewing-angle dependence. Given the qualitatively different evolution we find in the blue and red optical bands, it will also be valuable to extend this analysis to ultraviolet and infrared wavelengths, where the contrast between BNS and NSBH KNe may be even more pronounced. Ultimately, the strongest assessment will require an apples-to-apples comparison of BNS and NSBH mergers using high-resolution general relativistic magnetohydrodynamic simulations and consistent post-processing pipelines, to determine whether

the separation we identify in the post-peak decline distribution persists in more complete models. If it does, KN light curves will offer a new way to connect EM transients to their progenitors and, in turn, to the astrophysics of compact binary mergers.

CONTRIBUTIONS

IG led the project and carried out the large-scale simulations for BNS and NSBH population models. IG, YB, and RK analyzed the simulation outputs and generated the key figures. RK developed the Python code used to compute kilonova light curves, based on literature prescriptions identified with input from MB. The code was further refined by IG.

ACKNOWLEDGEMENTS

The authors acknowledge Wen-fai Fong and David Radice for useful discussions, and Sebastiano Bernuzzi for clarifications regarding the employed fits. IG acknowledges support from the Network for Neutrinos, Nuclear Astrophysics, and Symmetries (N3AS) Collaboration, NSF grant: PHY-2020275. IG also acknowledges the computational resources provided by the Gwave cluster, maintained by the Institute for Computational and Data Sciences at Penn State University, supported by NSF grants: OAC-2346596, OAC-2201445, OAC-2103662, OAC-2018299, and PHY-2110594. RK and YB acknowledge the support of Param Rudra, the high-performance computing facility established under the National Supercomputing Mission at IIT Bombay. YB also acknowledges the LIGO Lab computational resources, supported by NSF grants: PHY-0757058 and PHY-0823459. Parts of this work are included in YB's Master's thesis project at IIT Bombay. MB acknowledges support from the Eberly Research Fellowship at the Pennsylvania State University and the Simons Collaboration on Extreme Electrodynamics of Compact Sources (SCEECs) Postdoctoral Fellowship at the Wisconsin IceCube Particle Astrophysics Center (WIPAC), University of Wisconsin-Madison.

DATA AVAILABILITY

The data underlying this article will be shared on reasonable request to the corresponding author.

APPENDIX

A. DETAILED DESCRIPTION OF KILONOVA MODELING

A.1. Fits from numerical relativity simulations

The matter content of the viscous or neutrino-driven wind and dynamical ejecta for BNS/NSBH mergers is determined by their binary parameters. Although numerical relativity simulations are required to accurately predict the ejecta masses for these mergers, here we adopt analytical expressions inferred from numerical simulations that cover a broad range of binary parameters.

A.1.1. Fits for BNS mergers

For BNS mergers, the dynamical ejecta mass is estimated by (Radice et al. 2018a; Dietrich & Ujevic 2017; Kawaguchi et al. 2016)

$$\frac{M_{\text{dyn}}^{\text{BNS}}}{10^{-3}M_{\odot}} = \left[\alpha \left(\frac{M_2}{M_1} \right)^{1/3} \left(\frac{1 - 2C_1}{C_1} \right) + \beta \left(\frac{M_2}{M_1} \right)^n + \gamma \left(1 - \frac{M_1}{M_{b,1}} \right) \right] M_{b,1} + (1 \leftrightarrow 2) + \delta, \quad (\text{A1})$$

where $C_i = GM_i/(R_i c^2)$ is the NS compactness corresponding to gravitational mass M_i and radius R_i , and $M_{b,i}$ is the baryonic mass of the NS. With the M0RefSet + M0/M1Set models with neutrino absorption and emission, Nedora et al. (2022) provides the fitting coefficients for $\log_{10} M_{\text{dyn}}^{\text{BNS}}$ as $\alpha = -0.1004$, $\beta = -0.4403$, $\gamma = -0.6452$, $\delta = 0.2696$, and $n = 0.3222$.

For the remnant disk mass, we use the analytical fit from Radice et al. (2018a), given by

$$\log_{10} \left(\frac{M_{\text{disk}}^{\text{BNS}}}{M_{\odot}} \right) = \max \left[-3.0, \log_{10} \left(\alpha + \beta \tanh \left(\frac{\tilde{\Lambda} - \gamma}{\delta} \right) \right) \right], \quad (\text{A2})$$

with $\alpha = 0.1206$, $\beta = 0.05095$, $\gamma = 471.0$, and $\delta = 0.5351$ (Nedora et al. 2022). Here, $\tilde{\Lambda}$ is the reduced tidal deformability parameter. 30% of this mass is chosen to contribute to disk wind, via neutrino-driven winds and viscous ejecta components.

The total unbound ejecta is calculated as the sum of the dynamical ejecta and disk wind. Following the three-component model in Villar et al. (2017), we attribute 20% of the total ejecta to the red and blue components each, and the remaining 60% to the purple component (cf. Section 2).

The velocity of the ejecta is given by (Radice et al. 2018a; Dietrich & Ujevic 2017),

$$v/c = \left[\alpha \left(\frac{M_1}{M_2} \right) (1 + \gamma C_1) \right] + (1 \leftrightarrow 2) + \beta, \quad (\text{A3})$$

with $\alpha = -0.5631$, $\beta = 1.109$, and $\gamma = -1.186$ (Nedora et al. 2022).

We note that the conclusions of this work can depend sensitively on the fitting formulae used to estimate the ejecta masses. These fits can incur substantial errors and, in some cases, may be ill-conditioned (Nedora et al. 2022). For e.g., in the disk mass fit of Eq. A2, the best-fit value $\delta = 0.5351$ implies that for nearly all values of $\tilde{\Lambda}$ differing from $\gamma = 471$ by more than ~ 2 , the argument of the hyperbolic tangent saturates, such that $\tanh[(\tilde{\Lambda} - \gamma)/\delta] \approx \pm 1$. As a result, the inferred disk masses for the BNS population cluster into two preferred branches. This feature propagates directly into the KN light curves and is responsible for the bimodality seen in the BNS post-peak decline distributions in Section 3.

To assess the sensitivity of our results to this modeling choice, we repeat the analysis using an alternative set of fitting formulae for the BNS dynamical and disk ejecta from Krüger & Foucart (2020). The dynamical ejecta mass is given by

$$\frac{M_{\text{dyn}}^{\text{BNS}}}{10^{-3}M_{\odot}} = \left(\frac{\alpha}{C_1} + \beta \left(\frac{M_2}{M_1} \right)^n + \gamma C_1 \right) M_1 + (1 \leftrightarrow 2), \quad (\text{A4})$$

where $\alpha = -1.261 \times 10^{-3}$, $\beta = 1.449 \times 10^{-2}$, $\gamma = -4.715 \times 10^{-2}$, and $n = 1.306$ (Nedora et al. 2022). The disk mass is estimated as

$$\log_{10} \left(\frac{M_{\text{disk}}^{\text{BNS}}}{M_{\odot}} \right) = \log_{10} M_1 + \max(-3.3, \gamma \log_{10}(\alpha C_{\text{NS},1} + \beta)), \quad (\text{A5})$$

where $\alpha = -7.184$, $\beta = 1.303$, and $\gamma = 1.613$ (Nedora et al. 2022). Unlike Eq. A2, this prescription avoids the artificial saturation induced by the hyperbolic tangent. However, it predicts negligible disk ejecta for primaries with moderate

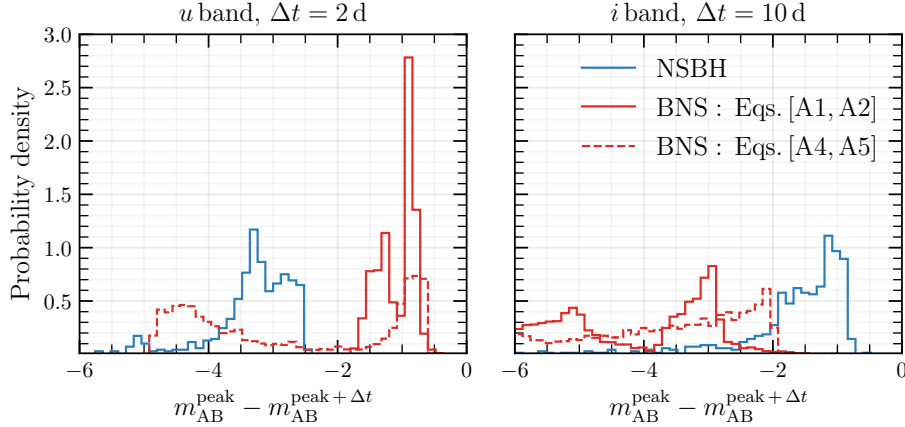


Figure 5. Comparison of the post-peak decline distributions obtained using two different prescriptions for the BNS ejecta masses, for the fiducial “Uniform” BNS and NSBH populations with the DD2 EOS. The alternative BNS fits in Eqs. A4 and A5 remove the bimodality introduced by the tanh disk mass fit used in the main text, but also impose an effective floor on the disk ejecta for sufficiently compact primary NSs. The new fits shift the BNS distribution toward slower-declining light curves in the i band for low-mass systems. In the u band, they produce a bimodal BNS distribution: slowly declining light curves from low-mass NS binaries, and a rapidly decaying branch from systems with $M_1 \gtrsim 1.6 M_\odot$ whose disk ejecta masses collapse to the fit floor. Since this floor reflects numerical uncertainty in the underlying simulations (Krüger & Foucart 2020), the rapidly decaying u band branch should not be interpreted as physical.

to high compactness, approaching a floor of $M_{\text{disk}}^{\text{BNS}} \simeq 5 \times 10^{-4} M_\odot$ for $C_1 \gtrsim 0.18$. This floor reflects the calibration uncertainty of the fit rather than a robust physical prediction for the disk mass (Krüger & Foucart 2020).

Figure 5 compares the fiducial “Uniform” BNS and NSBH populations, assuming the DD2 EOS, in the u and i band post-peak decline distributions when the alternative BNS ejecta fits of Eqs. A4 and A5 are used in place of the baseline prescription adopted in the main analysis. The new fits predict larger disk ejecta masses for low mass NSs, which shifts part of the BNS distribution rightward in the i band, toward more slowly declining KNe. This increases the overlap with the fiducial NSBH population, although a substantial fraction of NSBH mergers still occupies the more slowly evolving region.

In the u band, the effect is more pronounced. With the alternative fits, one branch of the BNS distribution moves closer to negligible ($\lesssim 0.5$ mag) decline, corresponding to very slowly evolving blue emission, while a second branch peaks near -5 , indicating much more rapid fading. This rapidly declining branch comprises systems with $M_1 \gtrsim 1.6 M_\odot$, for which the inferred disk mass is driven to the floor value of $\sim 5 \times 10^{-4} M_\odot$. Consequently, although these systems appear to overlap with NSBH mergers in the post-peak decline distribution, this overlap is an artifact of the fit reaching its calibration floor rather than a robust physical prediction.

As expected, the quantitative degree of separation between BNS and NSBH KNe depends on the ejecta fits adopted. More generally, fits that predict larger BNS ejecta masses lead to slower declining ejecta in the u and i bands. This tends to move the BNS and NSBH post-peak decline distributions closer together in the i band, while increasing their separation in the u band; fits that predict smaller ejecta masses tend to have the opposite effect. Thus, the precise amount of overlap between the two merger classes is fit-dependent. Nevertheless, even under these alternative prescriptions, BNS and NSBH KNe remain reasonably separable in one or more of the regions of parameter space identified in this work.

A.1.2. Fits for NSBH mergers

Depending on the initial BH and NS parameters, the outcome of an NSBH merger can be two-fold: either the NS plunges directly into the BH before it can be tidally disrupted, or the tidal forces on the NS become strong enough to disrupt it before it reaches ISCO. The binary parameters that determine this outcome are the binary mass ratio $q = M_{\text{BH}}/M_{\text{NS}}$ (Kyutoku et al. 2011; Foucart et al. 2012), BH spin magnitude a_{BH} and orientation (Pannarale et al. 2011; Foucart 2012), and NS radius R_{NS} , given by the EOS (Duez et al. 2010; Kyutoku et al. 2010). NS tidal disruption by BH is facilitated by a larger R_{NS} (for smaller C_{NS}), smaller M_{BH} and/or larger χ_{BH} . The amount of NS material

ejected before falling into the BH is determined by the relative positions of the tidal disruption radius and the ISCO radius, where the latter is given by

$$\frac{R_{\text{ISCO}}}{M_{\text{BH}}} = 3 + Z_2 - \text{sign}(\chi_{\text{BH}}) \sqrt{(3 - Z_1)(3 + Z_1 + 2Z_2)} \quad (\text{A6})$$

where $Z_1 = 1 + (1 - \chi_{\text{BH}}^2)^{1/3} [(1 + \chi_{\text{BH}})^{1/3} + (1 - \chi_{\text{BH}})^{1/3}]$ and $Z_2 = \sqrt{3\chi_{\text{BH}}^2 + Z_1^2}$.

Krüger & Foucart (2020) estimated the mass of NSBH dynamical ejecta with the analytical fit

$$\frac{M_{\text{dyn}}^{\text{NSBH}}}{M_{\text{b,NS}}} = a_1 q^{n_1} \left(\frac{1 - 2C_{\text{NS}}}{C_{\text{NS}}} \right) - a_2 q^{n_2} \frac{R_{\text{ISCO}}}{M_{\text{BH}}} + a_3, \quad (\text{A7})$$

where $a_1 = 0.007116$, $a_2 = 0.001436$, $a_3 = -0.02762$, $n_1 = 0.8636$, and $n_2 = 1.6840$ are the best-fit parameters. Here, $M_{\text{b,NS}}$ is the NS baryonic mass, and C_{NS} is its compactness. Negative values obtained from equation (A7) represent no dynamical mass ejected post NSBH merger. Foucart et al. (2017) estimated the average velocity of dynamical ejecta as $v_{\text{dyn}}^{\text{NSBH}} = (0.0149q + 0.1493)c$.

Foucart et al. (2018) provides the following fit for the remaining baryonic mass outside the remnant BH ~ 10 ms after merger:

$$\frac{M_{\text{rem}}^{\text{NSBH}}}{M_{\text{b,NS}}} = \max \left[\left(\alpha \frac{1 - 2C_{\text{NS}}}{\eta^{1/3}} - \beta \frac{R_{\text{ISCO}}}{M_{\text{BH}}} \frac{C_{\text{NS}}}{\eta} + \gamma \right)^\delta, 0 \right] \quad (\text{A8})$$

where $\alpha = 0.406$, $\beta = 0.139$, $\gamma = 0.255$, $\delta = 1.761$ are fit parameters, and $\eta = q/(1+q)^2$, also referred to as the symmetric mass ratio. $M_{\text{dyn}}^{\text{NSBH}}$ and $M_{\text{rem}}^{\text{NSBH}}$ are found to be larger for a smaller M_{BH} , larger a_{BH} and stiffer NS EOS (i.e., smaller C_{NS}). The mass of the NSBH accretion disk is estimated using $M_{\text{disk}}^{\text{NSBH}} = M_{\text{rem}}^{\text{NSBH}} - M_{\text{dyn}}^{\text{NSBH}}$. A significant portion of this disk can become gravitationally unbound through outflows that are either thermally or magnetically driven. The mass loss due to NSBH disk wind can be estimated as (Fernández et al. 2020),

$$\frac{M_{\text{wind}}^{\text{NSBH}}}{M_{\text{disk}}^{\text{NSBH}}} = \xi_1 + \frac{\xi_2 - \xi_1}{1 + e^{1.5(q-3)}}, \quad (\text{A9})$$

where we assume average values for the free parameters $\xi_1 = 0.18$ and $\xi_2 = 0.29$ (Raaijmakers et al. 2021).

Unlike dynamical ejecta for NSBH mergers, winds originating from the remnant accretion disk are expected to be spherically symmetric. Although the velocity of the disk wind ejecta is quite uncertain, recent simulations have shown that the velocity for bulk of the material is centered around $\sim 0.1c$ (Siegel & Metzger 2017; De & Siegel 2021; Fernández et al. 2020).

In Section 3.3, we also examine the effect of varying Y_e in the dynamical and disk wind ejecta relative to the fiducial values $Y_e = 0.1$ and 0.3 , respectively. Following Ekanger et al. (2023), we consider Y_e in the ranges $0.05 - 0.1$ for the dynamical ejecta and $0.1 - 0.5$ for the disk ejecta. Because the KN model takes the opacity as an input parameter, we map the assumed Y_e values to κ by fitting to the $Y_e - \kappa$ data of Tanaka et al. (2020). Our best-fit relation is

$$\kappa(Y_e) = 1.9469 + \frac{24.4696}{0.6991 + (4.6822 Y_e)^{7.8073}}. \quad (\text{A10})$$

This fit yields a smooth decrease in κ to $\sim 2 \text{ cm}^2 \text{ g}^{-1}$ at $Y_e \sim 0.5$, while approaching $\kappa \sim 38 \text{ cm}^2 \text{ g}^{-1}$ for $Y_e \lesssim 0.05$. Under this mapping, $Y_e = \{0.05, 0.1, 0.3, 0.5\}$ corresponds to $\kappa = \{36.95, 36.82, 3.59, 1.98\} \text{ cm}^2 \text{ g}^{-1}$, respectively.

A.1.3. Obtaining bandwise light curves

After obtaining the ejecta masses and opacities, the heating rate \dot{Q} , as a function of time, is given by (Korobkin et al. 2012),

$$\dot{Q} = 4 \times 10^{18} \times M_{ej} \times \left(\frac{1}{2} - \frac{1}{\pi} \tan^{-1} \left(\frac{t - t_0}{s} \right) \right)^{1.3} \quad (\text{A11})$$

where M_{ej} is the ejecta mass, $t_0 = 1.3$ and $s = 0.11$. Together with the thermal efficiency, ϵ_{th} , obtained from Barnes et al. (2016), we approximate the bolometric light curve as,

$$L_{bol}(t) = 2 \exp \left(-\frac{t^2}{\tau^2} \right) \int_{t_i}^t \dot{Q}(t') \times \epsilon_{th}(t') \times \frac{t'}{\tau^2} \times \exp \left(\frac{t'^2}{\tau^2} \right) dt' \quad (\text{A12})$$

where $\tau = \sqrt{\tau_{diff}\tau_{exp}}$ (c.f. Section 2), and t_i is the initial time. To estimate the bandwise light curves from the bolometric luminosity, we model the emission as a blackbody with photospheric temperature T and radius R . The photosphere expands with the ejecta as $R = v_{ej} \times t$, where v_{ej} is the velocity of the ejecta. T and R characterize the associated spectral flux density f_ν :

$$f_\nu = \frac{2h\nu^3}{c^2} \frac{1}{e^{\frac{h\nu}{kT}} - 1} \left(\frac{R}{D_L} \right)^2, \quad (\text{A13})$$

where h is the Planck constant, ν is the frequency corresponding to the photometric band, k is the Boltzmann constant, and D_L is the luminosity distance of the system. Following Villar et al. (2017), we impose a temperature floor $T_c = 3000$ K to approximate the onset of recombination of elements to neutral (Barnes & Kasen 2013). Once the freely expanding ejecta cools below T_c , the photosphere radius recedes according to

$$R(t) = \left(\frac{L_{bol}(t)}{4\pi\sigma_{SB}T_c^4} \right)^{1/2}, \quad (\text{A14})$$

where σ_{SB} is the Stefan-Boltzmann constant. This captures the drop in opacity associated with the recombination. The color evolution remains constant in time, flattening the light curve, while the effective photosphere moves inward through the ejecta (Barnes & Kasen 2013).

The spectral flux can then be converted to AB magnitude m_{AB} using

$$m_{AB} = -2.5 \log_{10} f_\nu - 48.6. \quad (\text{A15})$$

For the *ugrizy* bands, we use the following wavelengths: $\lambda_u = 3.546 \times 10^{-7}$ m, $\lambda_g = 4.670 \times 10^{-7}$ m, $\lambda_r = 6.156 \times 10^{-7}$ m, $\lambda_i = 7.472 \times 10^{-7}$ m, $\lambda_z = 8.917 \times 10^{-7}$ m, and $\lambda_y = 1.0305 \times 10^{-6}$ m.

B. EFFECT OF BINARY PARAMETERS ON EJECTA PROPERTIES

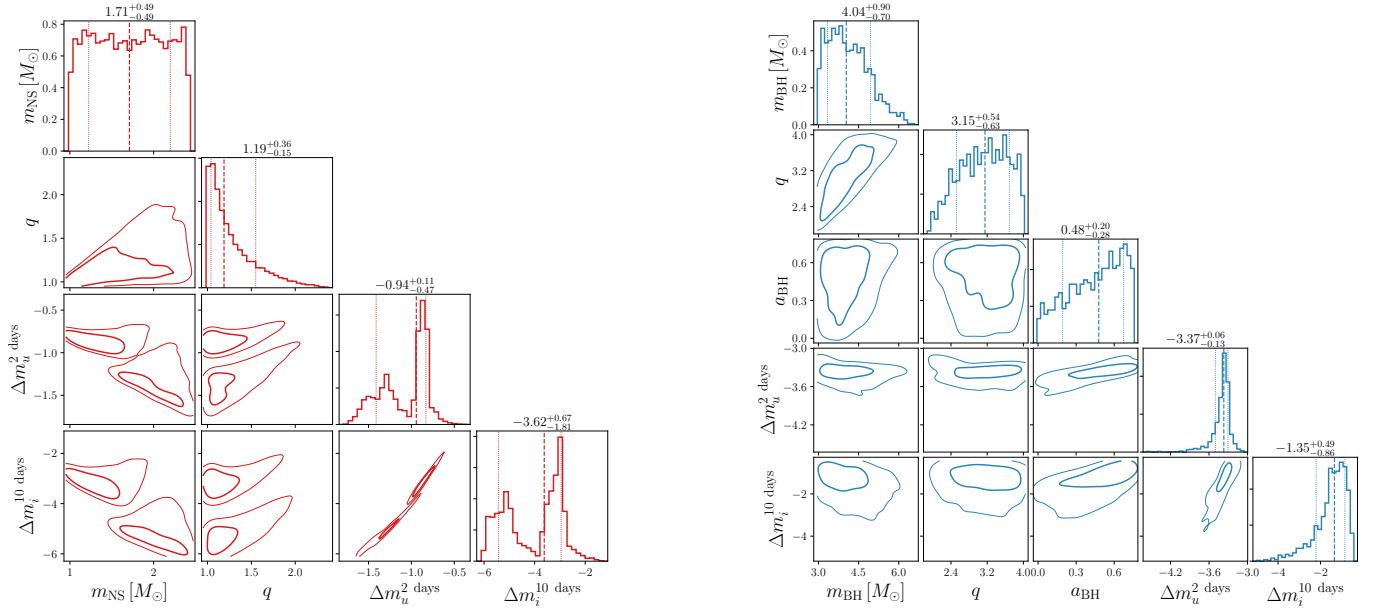


Figure 6. Dependence of the post-peak decline of KN light curves on the binary parameters for BNS (left) and NSBH (right) mergers. For BNS, the plot shows the relationship between the primary NS mass m_{NS} , the binary mass ratio q , and the post-peak decline in the u and i bands. For NSBHs, we show the dependence of post-peak decline in the two bands with the mass of the BH m_{BH} , q , and the dimensionless spin of the BH a_{BH} . For both merger classes, results are shown for the fiducial “Uniform” population and the DD2 EOS. The plotted distributions illustrate how the decline rates in the u and i bands correlate with the binary masses and, for NSBH mergers, also with the BH spin.

Figure 6 illustrates how the post-peak decline of the KN light curves depends on the underlying binary parameters. For BNS mergers, the figure shows the relation between the primary NS mass m_{NS} , the binary mass ratio q , and the

post-peak decline in the u band, $\Delta m_u^{2 \text{ days}}$, and the i band, $\Delta m_i^{10 \text{ days}}$. For NSBH mergers, we instead show how the same decline measures depend on the BH mass m_{BH} , the mass ratio q , and the dimensionless BH spin a_{BH} .

For BNS systems, lower mass NSs are less compact and more easily disrupted, yielding larger ejecta masses. This trend is reflected in the strong correlation between slowly declining u and i band light curves and low primary NS masses, $m_{\text{NS}} \lesssim 1.5 M_{\odot}$. Even when the primary NS is more massive, a sufficiently low mass companion can still lead to higher ejecta mass and produce slower post-peak evolution. This contributes to the trend with mass ratio, in which more asymmetric BNS mergers tend to decline more slowly in both bands. The same behavior is also consistent with numerical simulations showing that unequal-mass BNS mergers can produce more ejecta than nearly equal-mass systems (Camilletti et al. 2022).

For NSBH systems, the dominant parameters are the BH mass and spin. Smaller BH masses and larger aligned spins reduce R_{ISCO} and are conducive to tidal disruption, which in turn increases both the unbound ejecta and the remnant disk mass. This is clearly seen in Figure 6, where systems with lower m_{BH} (correspondingly, $q \gtrsim 0.5$) and higher a_{BH} , are strongly associated with slower decline in both the u and i bands.

An important feature is that the post-peak decline remains well-separated even when the mass parameters of BNS and NSBH systems become comparable, for e.g., between a low mass BH with $m_{\text{BH}} \sim 2.5 M_{\odot}$ and a high mass NS with $m_{\text{NS}} \sim 2.5 M_{\odot}$. In our models, the high mass NS configurations typically yield decline rates of $\Delta m_u^{2 \text{ days}} \sim -1.75$ and $\Delta m_i^{10 \text{ days}} \sim -6$, whereas the low-mass BH configurations give markedly different values of $\Delta m_u^{2 \text{ days}} \sim -3.25$ and $\Delta m_i^{10 \text{ days}} \sim -1$. At current and near-future GW detector sensitivities, such low mass BHs can be difficult to distinguish from high mass NSs using GW information alone (Golomb et al. 2024; Dhani et al. 2025). Thus, the post-peak decline in photometric bands can provide an independent way to characterize such systems.

C. BANDWISE TEMPORAL EVOLUTION OF KNE

Figure 7 shows the post-peak decline distributions in the *ugrizy* bands for both BNS and NSBH KNe, evaluated 1, 2, 5, 10, and 15 d after peak. The bluer u band shows the clearest separation between the two merger classes at early times ($\Delta t < 5$ d), with the largest separation among the sampled time windows occurring 2 days after peak. As one moves to redder bands, the separation becomes more pronounced at later times, with the contrast between BNS and NSBH populations becoming especially clear for $\Delta t \gtrsim 5$ d. Motivated by these trends, in the main text, we use the u band decline 2 days after peak and the i band decline 10 days after peak as representative observables. More broadly, this behavior suggests that even bluer bands at early times, or redder bands at late times, may provide stronger separation between the two binary classes.

REFERENCES

- Abac, A., et al. 2025a. <https://arxiv.org/abs/2503.12263>
- Abac, A. G., et al. 2024, *Astrophys. J. Lett.*, 970, L34, doi: 10.3847/2041-8213/ad5beb
- . 2025b. <https://arxiv.org/abs/2508.18082>
- . 2025c. <https://arxiv.org/abs/2508.18083>
- Abbasi, R., et al. 2021. <https://arxiv.org/abs/2105.13160>
- Abbott, B. P., et al. 2017a, *Phys. Rev. Lett.*, 119, 161101, doi: 10.1103/PhysRevLett.119.161101
- . 2017b, *Astrophys. J. Lett.*, 848, L12, doi: 10.3847/2041-8213/aa91c9
- . 2017c, *Astrophys. J. Lett.*, 848, L13, doi: 10.3847/2041-8213/aa920c
- . 2017d, *Class. Quant. Grav.*, 34, 044001, doi: 10.1088/1361-6382/aa51f4
- . 2018, *Living Rev. Rel.*, 21, 3, doi: 10.1007/s41114-020-00026-9
- . 2020, *Astrophys. J. Lett.*, 892, L3, doi: 10.3847/2041-8213/ab75f5
- Abbott, R., et al. 2021, *Astrophys. J. Lett.*, 915, L5, doi: 10.3847/2041-8213/ac082e
- Akmal, A., Pandharipande, V. R., & Ravenhall, D. G. 1998, *Phys. Rev. C Nucl. Phys.*, 58, 1804, doi: 10.1103/PhysRevC.58.1804
- Alexander, K. D., et al. 2017, *Astrophys. J. Lett.*, 848, L21, doi: 10.3847/2041-8213/aa905d
- Anand, S., et al. 2021, *Nature Astron.*, 5, 46, doi: 10.1038/s41550-020-1183-3
- Andreoni, I., et al. 2022, *Astrophys. J. Supp.*, 260, 18, doi: 10.3847/1538-4365/ac617c
- . 2024, *Astropart. Phys.*, 155, 102904, doi: 10.1016/j.astropartphys.2023.102904
- Antoniadis, J., Tauris, T. M., Ozel, F., et al. 2016. <https://arxiv.org/abs/1605.01665>
- Arnett, D. 1982, *Astrophys. J.*
- Ashkar, H., Brun, F., Fückling, M., et al. 2021, *JCAP*, 03, 045, doi: 10.1088/1475-7516/2021/03/045

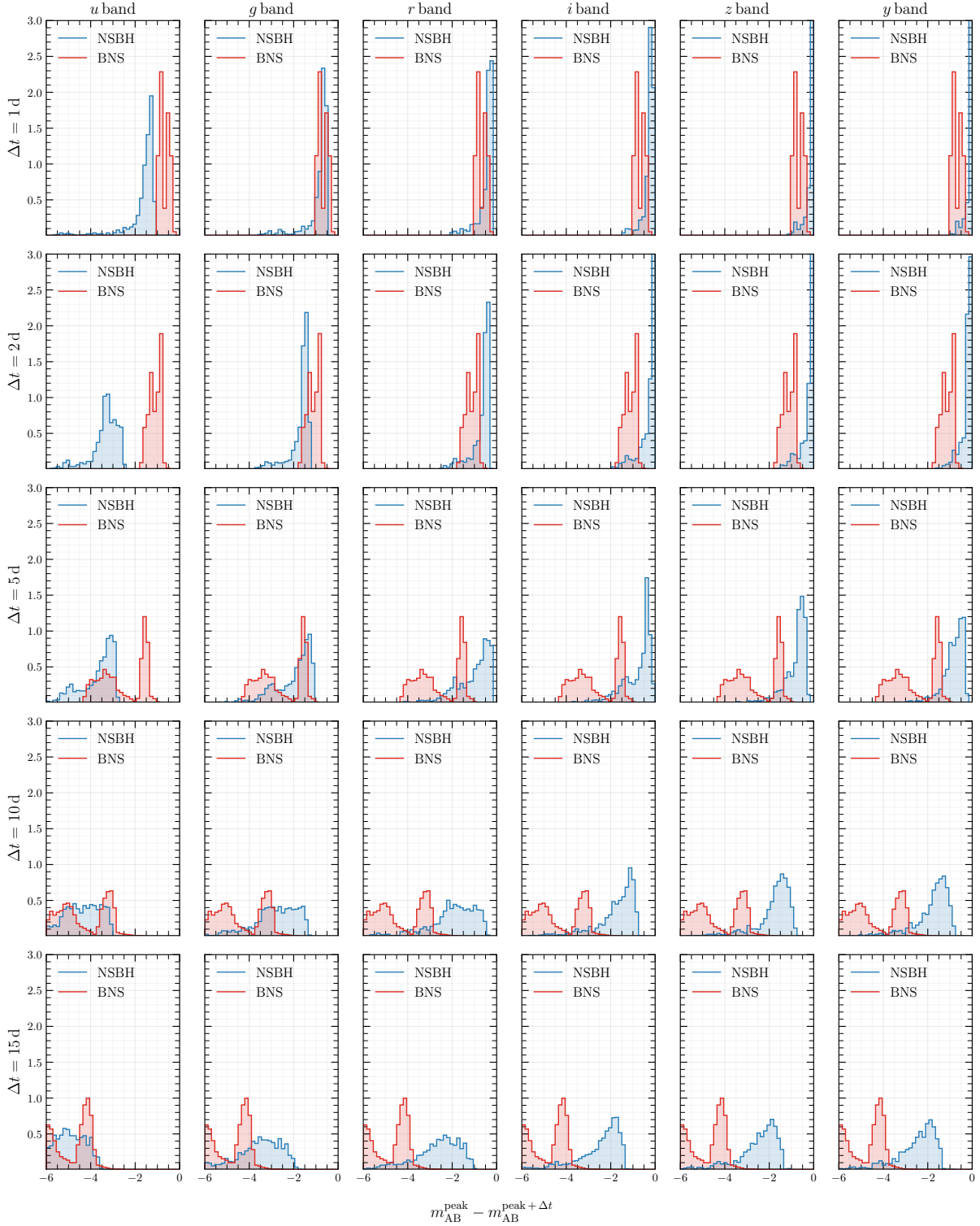


Figure 7. Post-peak decline distributions of BNS and NSBH KN light curves in the optical *ugrizy* bands, evaluated at $\Delta t = 1, 2, 5, 10,$ and 15 d after peak. For both merger classes, the astrophysical population is fixed to the fiducial “Uniform” prior and the EOS to DD2. The figure shows that the clearest separation appears in bluer bands at earlier times and in redder bands at later times, motivating the choice of the *u* band at 2 d after peak and the *i* band at 10 d after peak in the main text.

- Banik, S., Hempel, M., & Bandyopadhyay, D. 2014, *Astrophys. J. Suppl.*, 214, 22, doi: [10.1088/0067-0049/214/2/22](https://doi.org/10.1088/0067-0049/214/2/22)
- Barnes, J., & Kasen, D. 2013, *Astrophys. J.*, 775, 18, doi: [10.1088/0004-637X/775/1/18](https://doi.org/10.1088/0004-637X/775/1/18)
- Barnes, J., Kasen, D., Wu, M.-R., & Martínez-Pinedo, G. 2016, *Astrophys. J.*, 829, 1, doi: [10.3847/0004-637X/829/2/110](https://doi.org/10.3847/0004-637X/829/2/110)
- Bhattacharya, M., Kumar, P., & Smoot, G. 2019, *Mon. Not. Roy. Astron. Soc.*, 486, 5289, doi: [10.1093/mnras/stz1147](https://doi.org/10.1093/mnras/stz1147)
- Biscoveanu, S., Landry, P., & Vitale, S. 2022, *Mon. Not. Roy. Astron. Soc.*, 518, 5298, doi: [10.1093/mnras/stac3052](https://doi.org/10.1093/mnras/stac3052)
- Borhanian, S., & Sathyaprakash, B. S. 2024, *Phys. Rev. D*, 110, 083040, doi: [10.1103/PhysRevD.110.083040](https://doi.org/10.1103/PhysRevD.110.083040)
- Branchesi, M., et al. 2023, *JCAP*, 07, 068, doi: [10.1088/1475-7516/2023/07/068](https://doi.org/10.1088/1475-7516/2023/07/068)
- Breschi, M., Perego, A., Bernuzzi, S., et al. 2021, *Mon. Not. Roy. Astron. Soc.*, 505, 1661, doi: [10.1093/mnras/stab1287](https://doi.org/10.1093/mnras/stab1287)
- Brethauer, D., Kasen, D., Margutti, R., & Chornock, R. 2024, *Astrophys. J.*, 975, 213, doi: [10.3847/1538-4357/ad7d83](https://doi.org/10.3847/1538-4357/ad7d83)
- Bulla, M. 2023, *Mon. Not. Roy. Astron. Soc.*, 520, 2558, doi: [10.1093/mnras/stad232](https://doi.org/10.1093/mnras/stad232)
- Camilletti, A., Chiesa, L., Ricigliano, G., et al. 2022, *Mon. Not. Roy. Astron. Soc.*, 516, 4760, doi: [10.1093/mnras/stac2333](https://doi.org/10.1093/mnras/stac2333)
- Chandra, K., Gupta, I., Gamba, R., et al. 2024, *Astrophys. J.*, 977, 167, doi: [10.3847/1538-4357/ad90bd](https://doi.org/10.3847/1538-4357/ad90bd)
- Chase, E. A., O'Connor, B., Fryer, C. L., et al. 2022, *Astrophys. J.*, 927, 163, doi: [10.3847/1538-4357/ac3d25](https://doi.org/10.3847/1538-4357/ac3d25)
- Chattopadhyay, D., Stevenson, S., Broekgaarden, F., Antonini, F., & Belczynski, K. 2022, *Mon. Not. Roy. Astron. Soc.*, 513, 5780, doi: [10.1093/mnras/stac1283](https://doi.org/10.1093/mnras/stac1283)
- Chattopadhyay, D., Stevenson, S., Hurley, J. R., Bailes, M., & Broekgaarden, F. 2021, *Mon. Not. Roy. Astron. Soc.*, 504, 3682, doi: [10.1093/mnras/stab973](https://doi.org/10.1093/mnras/stab973)
- Chatzopoulos, E., Craig Wheeler, J., & Vinko, J. 2012, doi: [10.1088/0004-637X/746/2/121](https://doi.org/10.1088/0004-637X/746/2/121)
- Chaudhary, S. S., et al. 2024, *Proc. Nat. Acad. Sci.*, 121, e2316474121, doi: [10.1073/pnas.2316474121](https://doi.org/10.1073/pnas.2316474121)
- Chornock, R., et al. 2017, *Astrophys. J. Lett.*, 848, L19, doi: [10.3847/2041-8213/aa905c](https://doi.org/10.3847/2041-8213/aa905c)
- Cowperthwaite, P. S., Villar, V. A., Scolnic, D. M., & Berger, E. 2019, *Astrophys. J.*, 874, 88, doi: [10.3847/1538-4357/ab07b6](https://doi.org/10.3847/1538-4357/ab07b6)
- Cowperthwaite, P. S., et al. 2017, *Astrophys. J. Lett.*, 848, L17, doi: [10.3847/2041-8213/aa8fc7](https://doi.org/10.3847/2041-8213/aa8fc7)
- Darbha, S., & Kasen, D. 2020, 897, 150, doi: [10.3847/1538-4357/ab9a34](https://doi.org/10.3847/1538-4357/ab9a34)
- De, S., & Siegel, D. M. 2021, *Astrophys. J.*, 921, 94, doi: [10.3847/1538-4357/ac110b](https://doi.org/10.3847/1538-4357/ac110b)
- Dhani, A., Camilletti, A., Radice, D., et al. 2025, 112, 124003, doi: [10.1103/2yng-919s](https://doi.org/10.1103/2yng-919s)
- Dietrich, T., & Ujevic, M. 2017, *Class. Quant. Grav.*, 34, 105014, doi: [10.1088/1361-6382/aa6bb0](https://doi.org/10.1088/1361-6382/aa6bb0)
- Douchin, F., & Haensel, P. 2001, *Astron. Astrophys.*, 380, 151, doi: [10.1051/0004-6361:20011402](https://doi.org/10.1051/0004-6361:20011402)
- Duez, M. D., Foucart, F., Kidder, L. E., Ott, C. D., & Teukolsky, S. A. 2010, *Class. Quant. Grav.*, 27, 114106, doi: [10.1088/0264-9381/27/11/114106](https://doi.org/10.1088/0264-9381/27/11/114106)
- Eichler, D., Livio, M., Piran, T., & Schramm, D. N. 1989, *Nature*, 340, 126, doi: [10.1038/340126a0](https://doi.org/10.1038/340126a0)
- Ekanger, N., Bhattacharya, M., & Horiuchi, S. 2023, *Mon. Not. Roy. Astron. Soc.*, 525, 2040, doi: [10.1093/mnras/stad2348](https://doi.org/10.1093/mnras/stad2348)
- Evans, M., et al. 2023. <https://arxiv.org/abs/2306.13745>
- Fairhurst, S. 2011, *Class. Quant. Grav.*, 28, 105021, doi: [10.1088/0264-9381/28/10/105021](https://doi.org/10.1088/0264-9381/28/10/105021)
- Farrow, N., Zhu, X.-J., & Thrane, E. 2019, *Astrophys. J.*, 876, 18, doi: [10.3847/1538-4357/ab12e3](https://doi.org/10.3847/1538-4357/ab12e3)
- Fernández, R., Foucart, F., & Lippuner, J. 2020, *Mon. Not. Roy. Astron. Soc.*, 497, 3221, doi: [10.1093/mnras/staa2209](https://doi.org/10.1093/mnras/staa2209)
- Fong, W., et al. 2017, *Astrophys. J. Lett.*, 848, L23, doi: [10.3847/2041-8213/aa9018](https://doi.org/10.3847/2041-8213/aa9018)
- Foucart, F. 2012, *Phys. Rev. D*, 86, 124007, doi: [10.1103/PhysRevD.86.124007](https://doi.org/10.1103/PhysRevD.86.124007)
- Foucart, F., Duez, M. D., Kidder, L. E., et al. 2012, *Phys. Rev. D*, 85, 044015, doi: [10.1103/PhysRevD.85.044015](https://doi.org/10.1103/PhysRevD.85.044015)
- Foucart, F., Hinderer, T., & Nissanke, S. 2018, *Phys. Rev. D*, 98, 081501, doi: [10.1103/PhysRevD.98.081501](https://doi.org/10.1103/PhysRevD.98.081501)
- Foucart, F., Desai, D., Brege, W., et al. 2017, *Class. Quant. Grav.*, 34, 044002, doi: [10.1088/1361-6382/aa573b](https://doi.org/10.1088/1361-6382/aa573b)
- Golomb, J., Legred, I., Chatziioannou, K., Abac, A., & Dietrich, T. 2024, *Phys. Rev. D*, 110, 063014, doi: [10.1103/PhysRevD.110.063014](https://doi.org/10.1103/PhysRevD.110.063014)
- Gottlieb, O., Metzger, B. D., Quataert, E., et al. 2023, *Astrophys. J. Lett.*, 958, L33, doi: [10.3847/2041-8213/ad096e](https://doi.org/10.3847/2041-8213/ad096e)
- Gupta, I. 2023, *Mon. Not. Roy. Astron. Soc.*, 524, 3537, doi: [10.1093/mnras/stad2115](https://doi.org/10.1093/mnras/stad2115)
- . 2024, *Astrophys. J.*, 970, 12, doi: [10.3847/1538-4357/ad49a0](https://doi.org/10.3847/1538-4357/ad49a0)
- Gupta, I., Borhanian, S., Dhani, A., et al. 2023, *Phys. Rev. D*, 107, 124007, doi: [10.1103/PhysRevD.107.124007](https://doi.org/10.1103/PhysRevD.107.124007)
- Gupta, I., et al. 2024, *Class. Quant. Grav.*, 41, 245001, doi: [10.1088/1361-6382/ad7b99](https://doi.org/10.1088/1361-6382/ad7b99)

- Gutiérrez, E. M., Bhattacharya, M., Radice, D., Murase, K., & Bernuzzi, S. 2025, *Phys. Rev. D*, 111, 063031, doi: [10.1103/PhysRevD.111.063031](https://doi.org/10.1103/PhysRevD.111.063031)
- Heinzel, J., Coughlin, M. W., Dietrich, T., et al. 2020
- Hild, S., et al. 2011, *Class. Quant. Grav.*, 28, 094013, doi: [10.1088/0264-9381/28/9/094013](https://doi.org/10.1088/0264-9381/28/9/094013)
- Hounsell, R., et al. 2018, *Astrophys. J.*, 867, 23, doi: [10.3847/1538-4357/aac08b](https://doi.org/10.3847/1538-4357/aac08b)
- Ivezić, Ž., et al. 2019, *Astrophys. J.*, 873, 111, doi: [10.3847/1538-4357/ab042c](https://doi.org/10.3847/1538-4357/ab042c)
- Just, O., Bauswein, A., Pulpillo, R. A., Goriely, S., & Janka, H. T. 2015, *Mon. Not. Roy. Astron. Soc.*, 448, 541, doi: [10.1093/mnras/stv009](https://doi.org/10.1093/mnras/stv009)
- Kashyap, R., Raman, G., & Ajith, P. 2019, *Astrophys. J. Lett.*, 886, L19, doi: [10.3847/2041-8213/ab543f](https://doi.org/10.3847/2041-8213/ab543f)
- Kasliwal, M. M., et al. 2020, *Astrophys. J.*, 905, 145, doi: [10.3847/1538-4357/abc335](https://doi.org/10.3847/1538-4357/abc335)
- Kawaguchi, K., Kyutoku, K., Shibata, M., & Tanaka, M. 2016, *Astrophys. J.*, 825, 52, doi: [10.3847/0004-637X/825/1/52](https://doi.org/10.3847/0004-637X/825/1/52)
- Klion, H., Duffell, P. C., Kasen, D., & Quataert, E. 2020
- Korobkin, O., Rosswog, S., Arcones, A., & Winteler, C. 2012, *Mon. Not. R. Astron. Soc.*, 426, 1940, doi: [10.1111/j.1365-2966.2012.21859.x](https://doi.org/10.1111/j.1365-2966.2012.21859.x)
- Krüger, C. J., & Foucart, F. 2020, *Phys. Rev. D*, 101, 103002, doi: [10.1103/PhysRevD.101.103002](https://doi.org/10.1103/PhysRevD.101.103002)
- Kulkarni, S. R. 2005. <https://arxiv.org/abs/astro-ph/0510256>
- Kunnumkai, K., Palmese, A., Bulla, M., et al. 2025, *Phys. Rev. D*, 112, 123005, doi: [10.1103/dnjl-gc4x](https://doi.org/10.1103/dnjl-gc4x)
- Kyutoku, K., Okawa, H., Shibata, M., & Taniguchi, K. 2011, *Phys. Rev. D*, 84, 064018, doi: [10.1103/PhysRevD.84.064018](https://doi.org/10.1103/PhysRevD.84.064018)
- Kyutoku, K., Shibata, M., & Taniguchi, K. 2010, *Phys. Rev. D*, 82, 044049, doi: [10.1103/PhysRevD.82.044049](https://doi.org/10.1103/PhysRevD.82.044049)
- Lattimer, J. M., & Schramm, D. N. 1974, *Astrophys. J. Lett.*, 192, L145, doi: [10.1086/181612](https://doi.org/10.1086/181612)
- Li, L.-X., & Paczyński, B. 1998, *arXiv [astro-ph]*, L59, doi: [10.1086/311680](https://doi.org/10.1086/311680)
- Lippuner, J., Fernández, R., Roberts, L. F., et al. 2017, *Mon. Not. Roy. Astron. Soc.*, 472, 904, doi: [10.1093/mnras/stx1987](https://doi.org/10.1093/mnras/stx1987)
- Magee, R., et al. 2021, *Astrophys. J. Lett.*, 910, L21, doi: [10.3847/2041-8213/abed54](https://doi.org/10.3847/2041-8213/abed54)
- Margutti, R., et al. 2017, *Astrophys. J. Lett.*, 848, L20, doi: [10.3847/2041-8213/aa9057](https://doi.org/10.3847/2041-8213/aa9057)
- Metzger, B. D. 2020, *Living Rev. Rel.*, 23, 1, doi: [10.1007/s41114-019-0024-0](https://doi.org/10.1007/s41114-019-0024-0)
- Metzger, B. D., Martinez-Pinedo, G., Darbha, S., et al. 2010, *Mon. Not. Roy. Astron. Soc.*, 406, 2650, doi: [10.1111/j.1365-2966.2010.16864.x](https://doi.org/10.1111/j.1365-2966.2010.16864.x)
- Miller, J., Barsotti, L., Vitale, S., et al. 2015, *Phys. Rev. D*, 91, 062005, doi: [10.1103/PhysRevD.91.062005](https://doi.org/10.1103/PhysRevD.91.062005)
- Narayan, R., Paczynski, B., & Piran, T. 1992, *ApJL*, 395, L83, doi: [10.1086/186493](https://doi.org/10.1086/186493)
- Nedora, V., Schianchi, F., Bernuzzi, S., et al. 2022, *Class. Quant. Grav.*, 39, 015008, doi: [10.1088/1361-6382/ac35a8](https://doi.org/10.1088/1361-6382/ac35a8)
- Nicholl, M., et al. 2017, *Astrophys. J. Lett.*, 848, L18, doi: [10.3847/2041-8213/aa9029](https://doi.org/10.3847/2041-8213/aa9029)
- Özel, F., & Freire, P. 2016, *Ann. Rev. Astron. Astrophys.*, 54, 401, doi: [10.1146/annurev-astro-081915-023322](https://doi.org/10.1146/annurev-astro-081915-023322)
- Paek, G. S. H., et al. 2024, *Astrophys. J.*, 960, 113, doi: [10.3847/1538-4357/ad0238](https://doi.org/10.3847/1538-4357/ad0238)
- . 2025, *Astrophys. J.*, 981, 38, doi: [10.3847/1538-4357/adaf99](https://doi.org/10.3847/1538-4357/adaf99)
- Pannarale, F., Tonita, A., & Rezzolla, L. 2011, *Astrophys. J.*, 727, 95, doi: [10.1088/0004-637X/727/2/95](https://doi.org/10.1088/0004-637X/727/2/95)
- Paterson, K., et al. 2021, *Astrophys. J.*, 912, 128, doi: [10.3847/1538-4357/abeb71](https://doi.org/10.3847/1538-4357/abeb71)
- Phillips, M. M. 1993, *ApJL*, 413, L105, doi: [10.1086/186970](https://doi.org/10.1086/186970)
- Punturo, M., et al. 2010, *Class. Quant. Grav.*, 27, 194002, doi: [10.1088/0264-9381/27/19/194002](https://doi.org/10.1088/0264-9381/27/19/194002)
- Raaijmakers, G., et al. 2021, *Astrophys. J.*, 922, 269, doi: [10.3847/1538-4357/ac222d](https://doi.org/10.3847/1538-4357/ac222d)
- Radice, D., Bernuzzi, S., & Perego, A. 2020, *Ann. Rev. Nucl. Part. Sci.*, 70, 95, doi: [10.1146/annurev-nucl-013120-114541](https://doi.org/10.1146/annurev-nucl-013120-114541)
- Radice, D., Perego, A., Hotokezaka, K., et al. 2018a, *Astrophys. J.*, 869, 130, doi: [10.3847/1538-4357/aaf054](https://doi.org/10.3847/1538-4357/aaf054)
- Radice, D., Perego, A., Zappa, F., & Bernuzzi, S. 2018b, *Astrophys. J. Lett.*, 852, L29, doi: [10.3847/2041-8213/aaa402](https://doi.org/10.3847/2041-8213/aaa402)
- Rastinejad, J. C., et al. 2022, *Nature*, 612, 223, doi: [10.1038/s41586-022-05390-w](https://doi.org/10.1038/s41586-022-05390-w)
- Rees, M. J., & Mészáros, P. 1992, *Mon. Not. Roy. Astron. Soc.*, 258, 41P, doi: [10.1093/mnras/258.1.41P](https://doi.org/10.1093/mnras/258.1.41P)
- Reitze, D., et al. 2019, *Bull. Am. Astron. Soc.*, 51, 035. <https://arxiv.org/abs/1907.04833>
- Rezzolla, L., Baiotti, L., Giacomazzo, B., Link, D., & Font, J. A. 2010, *Class. Quant. Grav.*, 27, 114105, doi: [10.1088/0264-9381/27/11/114105](https://doi.org/10.1088/0264-9381/27/11/114105)
- Rezzolla, L., Giacomazzo, B., Baiotti, L., et al. 2011, *Astrophys. J. Lett.*, 732, L6, doi: [10.1088/2041-8205/732/1/L6](https://doi.org/10.1088/2041-8205/732/1/L6)
- Riess, A. G., et al. 1998, *Astron. J.*, 116, 1009, doi: [10.1086/300499](https://doi.org/10.1086/300499)
- Ronchini, S., et al. 2024, *Astrophys. J. Lett.*, 970, L20, doi: [10.3847/2041-8213/ad5d74](https://doi.org/10.3847/2041-8213/ad5d74)

- Sachdev, S., et al. 2020, *Astrophys. J. Lett.*, 905, L25, doi: [10.3847/2041-8213/abc753](https://doi.org/10.3847/2041-8213/abc753)
- Saleem, M., Chen, H.-Y., Siegel, D. M., et al. 2025. <https://arxiv.org/abs/2508.06020>
- Sari, R., Piran, T., & Narayan, R. 1998, *Astrophys. J. Lett.*, 497, L17, doi: [10.1086/311269](https://doi.org/10.1086/311269)
- Sarin, N., & Rosswog, S. 2024, *Astrophys. J. Lett.*, 973, L24, doi: [10.3847/2041-8213/ad739d](https://doi.org/10.3847/2041-8213/ad739d)
- Shingles, L. J., Collins, C. E., Vijayan, V., et al. 2023, 954, L41, doi: [10.3847/2041-8213/acf29a](https://doi.org/10.3847/2041-8213/acf29a)
- Siegel, D. M., & Metzger, B. D. 2017, *Phys. Rev. Lett.*, 119, 231102, doi: [10.1103/PhysRevLett.119.231102](https://doi.org/10.1103/PhysRevLett.119.231102)
- Soares-Santos, M., et al. 2017, *Astrophys. J. Lett.*, 848, L16, doi: [10.3847/2041-8213/aa9059](https://doi.org/10.3847/2041-8213/aa9059)
- Symbalisty, E., & Schramm, D. N. 1982, *Astrophys. Lett.*, 22, 143
- Tanaka, M., Kato, D., Gaigalas, G., & Kawaguchi, K. 2020, *Mon. Not. Roy. Astron. Soc.*, 496, 1369, doi: [10.1093/mnras/staa1576](https://doi.org/10.1093/mnras/staa1576)
- Tanvir, N. R., Levan, A. J., Fruchter, A. S., et al. 2013, *Nature*, 500, 547, doi: [10.1038/nature12505](https://doi.org/10.1038/nature12505)
- Thielemann, F. K., Eichler, M., Panov, I. V., & Wehmeyer, B. 2017, *Ann. Rev. Nucl. Part. Sci.*, 67, 253, doi: [10.1146/annurev-nucl-101916-123246](https://doi.org/10.1146/annurev-nucl-101916-123246)
- Villar, V. A., et al. 2017, *Astrophys. J. Lett.*, 851, L21, doi: [10.3847/2041-8213/aa9c84](https://doi.org/10.3847/2041-8213/aa9c84)
- Wijers, R. A. M. J., Rees, M. J., & Meszaros, P. 1997, *Mon. Not. Roy. Astron. Soc.*, 288, L51, doi: [10.1093/mnras/288.4.L51](https://doi.org/10.1093/mnras/288.4.L51)
- Wu, M.-R., Fernández, R., Martínez-Pinedo, G., & Metzger, B. D. 2016, *Mon. Not. Roy. Astron. Soc.*, 463, 2323, doi: [10.1093/mnras/stw2156](https://doi.org/10.1093/mnras/stw2156)
- Zhu, J.-P., Wang, X. I., Sun, H., et al. 2022, *Astrophys. J. Lett.*, 936, L10, doi: [10.3847/2041-8213/ac85ad](https://doi.org/10.3847/2041-8213/ac85ad)
- Zhu, J.-P., et al. 2021, *Astrophys. J.*, 917, 24, doi: [10.3847/1538-4357/abfe5e](https://doi.org/10.3847/1538-4357/abfe5e)
- . 2023, *Astrophys. J.*, 942, 88, doi: [10.3847/1538-4357/aca527](https://doi.org/10.3847/1538-4357/aca527)